



**HAL**  
open science

# Finite Difference preconditioning for compact scheme discretizations of the Poisson equation with variable coefficients

Stéphane Abide

► **To cite this version:**

Stéphane Abide. Finite Difference preconditioning for compact scheme discretizations of the Poisson equation with variable coefficients. *Journal of Computational and Applied Mathematics*, 2020, 379, pp.112872 -. 10.1016/j.cam.2020.112872 . hal-03490672

**HAL Id: hal-03490672**

**<https://hal.science/hal-03490672v1>**

Submitted on 22 Aug 2022

**HAL** is a multi-disciplinary open access archive for the deposit and dissemination of scientific research documents, whether they are published or not. The documents may come from teaching and research institutions in France or abroad, or from public or private research centers.

L'archive ouverte pluridisciplinaire **HAL**, est destinée au dépôt et à la diffusion de documents scientifiques de niveau recherche, publiés ou non, émanant des établissements d'enseignement et de recherche français ou étrangers, des laboratoires publics ou privés.



Distributed under a Creative Commons Attribution - NonCommercial 4.0 International License

# Finite Difference preconditioning for compact scheme discretizations of the Poisson equation with variable coefficients

Stéphane Abide

*Université de Perpignan Via Domitia, LAMPS EA 4217, Perpignan, France.*

---

## Abstract

The finite difference preconditioning for higher-order compact scheme discretizations of non separable Poisson's equation is investigated. [An eigenvalue analysis of a one-dimensional problem is detailed for compact schemes up to the tenth-order.](#) The analysis concludes that the spectrum is bounded irrespective of the mesh size and the continuous variable coefficient. Hence, combined to a multigrid method, the preconditioned Richardson method shows a convergence rate which is independent from the mesh size and the variable coefficient. Several numerical experiments, including the simulation of a flow with large density variations, confirm that the spectrum of the preconditioned operator remains bounded.

*Keywords:* Compact schemes, Poisson's equation, preconditioned Richardson method

---

## 1. Introduction

[The accurate numerical solution of the Poisson's equation is often required in the modeling of heat and mass transfer, in the presence of chemical reactions, in several scientific and engineering applications. The Poisson's equation may have constant or variable coefficients depending on the complexity of the problem. Accuracy and computational speed of the numerical solver can be improved by employing higher-order discretization within the framework of parallel methods. The development of such discretization and parallel methods for variable-coefficient Poisson's equation remains a challenge. In this work, a second-order](#)

---

*Email address:* [stephane.abide@univ-perp.fr](mailto:stephane.abide@univ-perp.fr) (Stéphane Abide)

15 finite-difference preconditioning method for higher-order compact schemes to solve the Pois-  
16 son's equation is developed and assessed for accuracy and computational performance.

17 One of the straightforward and popular methods to write a discretization of the vari-  
18 able coefficient Poisson equation is the common finite differences, elements or volumes. The  
19 resulting discrete Poisson operator is built on a *local* computational stencil and thus can  
20 benefit from efficient direct or iterative linear solvers at the cutting edge of the high perfor-  
21 mance computing [1–3] which permits to compute accurate solutions on fine grids. A recent  
22 comparative study of several Poisson solvers in an unit cube has been released by Gholami  
23 et al. [4] .

24 Another way to get accurate solution while limiting the number of degrees of freedom is  
25 to use higher-order discretizations. Spectral methods are these higher-order discretizations  
26 which exhibit an exponential decrease of the numerical error for sufficient regular solutions  
27 [5]. This strong property naturally leads authors to consider this discretization when com-  
28 puting accurate solution of benchmark problems [6]. Unlike lower-order discretizations, the  
29 *global* approximation of spectral methods introduces some specific difficulties: spurious oscil-  
30 lations due to a loss of local regularity conditions [7], large parallel communications inherent  
31 to FFT [8], and bad conditioning of discrete operators [5]. Orszag [9] proposed to use  
32 Finite- Difference preconditioning to achieve spectral accuracy with the Fourier spectral dis-  
33 cretization. Haldenwang et al. [10] discussed this approach regarding the Chebyshev spectral  
34 approximation. In both works, the theoretical analysis relies on the evaluation of the lowest  
35 and highest eigenvalues of the preconditioned discrete operator in the one-dimensional Pois-  
36 son equation. In addition to the derivation of the convergence rate bound  $\pi^2/4$ , Haldenwang  
37 et al. [10] has shown that the convergence rate is not sensitive to the boundary conditions and  
38 to the dimensionality of the problem. Always based on one-dimensional analysis Labrosse  
39 and Redondo [11] has presented a way to design an optimal lower-order preconditioner for  
40 the Chebyshev discretization of the Poisson 1d problem with a constant coefficient.

41 Other popular higher-order discretizations exist, such as the Higher-Order Compact  
42 Schemes. These Schemes are a set of higher-order finite differences achieving higher-order

43 accuracy on a small computational stencil [12–14]. One way to write such schemes is based  
44 on the substitution of the higher derivatives occurring in the central finite difference trun-  
45 cation error with [the](#) second-order finite difference approximation. This approach [has led](#) to  
46 the definition of the Mehrstellen scheme [12]. A large amount of works follows this [approach](#)  
47 [as illustrated](#) by the non-exhaustive selected papers [15–17]. One of the advantages [of pro-](#)  
48 [ceeding](#) in this way is that the resulting schemes lead to a sparse linear system irrespective  
49 to the problem [of](#) dimensionality, or [to more](#) general equations like convection/diffusion [18].  
50 Moreover, efficient iterative linear solvers like multigrid methods can benefit from the *local*  
51 computational stencil [17]. However, some [limits](#) may be outlined. First, the derivation of  
52 [such](#) schemes can be a tricky problem when non-uniform meshes or staggered grids have to  
53 be considered. Then, the derivation of such Mehrstellen-like schemes for the conservative  
54 formulation of a non-separable Poisson equation seems to remain an open issue. This con-  
55 servative formulation is still widely used to achieve conservation properties as for instance  
56 in computational fluid dynamics in order to enforce the divergence of the velocity.

57 [Another](#) way to derive HOCS discretization for Poisson’s equation [is to write](#) the problem  
58 in a tensorial form and then to write down the discretization in each direction [13]. This  
59 approach allows to consider [the](#) Poisson’s equation on staggered grids [19], [or to involve](#)  
60 variable coefficients [20]. [One of](#) the advantages of the one-dimensional HOCS is that the  
61 higher-order accuracy is achieved by solving tridiagonal or pentadiagonal linear systems.  
62 This former operation is performed with a linear algorithm complexity, even in parallel ar-  
63 chitecture [19]. [The drawback is, however,](#) that the resulting discrete Poisson operator is  
64 no longer sparse. The diagonalization method can be considered to compute solutions for  
65 this dense linear system [10]. Alternatively, iterative methods using a matrix free implemen-  
66 tation can be examined [as long as](#) the evaluation of the residual for the Poisson equation  
67 is performed with a linear complexity algorithm. But, the bad condition number inherent  
68 to the scheme accuracy needs to be reduced by using a specific preconditioner [21]. Abide  
69 and Zeghmati [19] [showed](#) that a common second-order finite difference preconditioning for  
70 the fourth-order compact scheme discretization of the two-dimensional constant coefficient

71 Poisson’s equation allows to bound the spectral radius independently to the mesh size.

72 The case of the non-separable Poisson’s equation is approached by several authors with  
73 methods similar to the defect correction [22]. The defect correction method introduces a  
74 simplified discrete operator, like lower-order discretization and/or constant coefficient, to  
75 determine successive corrections of the residual computed with the variable coefficient and  
76 eventually using high-order discretizations. This approach is investigated within the frame-  
77 work of the HOCS discretization of the constant coefficient Poisson equation on a staggered  
78 grid [19]. Nicoud [23] introduced a FD preconditioning based on a constant averaged co-  
79 efficient in the periodic directions to use a FFT-based Fast Poisson Solver. Within the  
80 framework of two-phase flows, Dodd and Ferrante [24] investigated a splitting, similar to  
81 the first step of the defect correction with a time-extrapolated initial guess for the pressure  
82 variable. This procedure is discussed and extended to HOCS discretizations in the context  
83 of the simulation of reactive flows based on the low Mach number approximation [25]. The  
84 deferred correction is also the strategy considered by Knikker [20] to tackle solutions of the  
85 HOCS discretization of Poisson’s equation. It is worth mentioning that regardless the dis-  
86 cretization scheme, the defect correction using a preconditioner based on an approximate  
87 coefficient constant Poisson’s equation has a convergence rate independent of the mesh-size,  
88 but dependent on the bound of the variable coefficients [26].

89 The present review outlines that the lower-order preconditioning of the spectral dis-  
90 cretization allows us to design iterative solvers that have a convergence rate independent of  
91 the mesh size [10]. A similar analysis for HOCS discretization established a similar result [19]  
92 in the case of constant coefficient Poisson’s equation. For the variable coefficient Poisson’s  
93 equation, the literature misses the analysis and the discussion of a such finite-difference pre-  
94 conditioning for HOCS discretizations. This is addressed by carrying out the computation of  
95 the condition number for the preconditioned Richardson iterative solver. The findings of this  
96 analysis are verified against several manufactured problems. The simulation flows involving  
97 large density gradients are also performed to verify and demonstrate the reliability of the  
98 lower-order finite difference preconditioning.

100 The next section presents the HOCS discretization of a non-separable Poisson's equation  
 101 written in a conservative form and defined on a staggered grid. The exact derivation of the  
 102 convergence rate for the Richardson method is established in the one-dimensional case for  
 103 the constant coefficient Poisson's equation. In the case of the variable coefficient, the spectral  
 104 radius is numerically computed and discussed. In the section 3, numerical experiments are  
 105 carried out to show that the conclusions of the eigenvalue analysis hold for multidimensional  
 106 problems. The conclusions are also verified against a test case of practical interest: the  
 107 simulation of the natural convection of air due to a large temperature gradient.

108

## 109 2. Analysis of the finite difference preconditioning

### 110 2.1. HOCS discretization of variable coefficient Poisson's equation

111 Let us consider the following non-separable Poisson's equation:

$$-\nabla \cdot (\kappa \nabla \phi) = f \quad (1)$$

112 where  $\kappa$  is a smooth variable coefficient and  $f$  the right hand side. Without loose of generality  
 113 the problem is defined on a cubical domain  $\Omega = [0, 1]^3$  for which Neumann or periodic bound-  
 114 ary conditions can be prescribed on the boundary  $\Gamma = \partial\Omega$ . This equation is the archetype  
 115 problem occurring in computational fluid dynamics, specifically with incompressible-like  
 116 models [20, 23] for which the divergence of the velocity have to be exactly enforced. The  
 117 present analysis focuses on this singular problem which it is known to be among the most  
 118 tricky part of incompressible-like solvers. So, as commonly encountered [with](#) the pressure-  
 119 like variable, the unknown  $\phi$  is cell-centered and the coefficient  $\kappa$  is face-centered. Regardless  
 120 the discretization, the finite difference approximation of Eq. (1) is formulated in a Cartesian  
 121 coordinates system as:

$$-\left(\delta_x^{fc} \bar{\kappa}^x \delta_x^{cf} + \delta_y^{fc} \bar{\kappa}^y \delta_y^{cf} + \delta_z^{fc} \bar{\kappa}^z \delta_z^{cf}\right) \phi = f \quad (2)$$

122 where  $\delta_\xi$  denotes the derivative operator in the  $\xi$ -direction, the superscript *fc* and *cf* refers  
 123 to *face-to-cell* and *cell-to-face* respectively. The notation  $\bar{\kappa}^\xi$  refers to the variable coefficient  
 124 evaluated at the faces in the  $\xi$ -direction. Let us define the uniform step size  $h_\xi = \ell_\xi/n_\xi$ , so  
 125 the cell and face centres are located at  $\xi_i = (i - 1/2)h_\xi$ ,  $0 \leq i \leq n_\xi + 1$  and  $\xi_{i+1/2} = i h_\xi$ ,  $0 \leq$   
 126  $i \leq n_\xi$ , respectively.

127 The discrete approximation of the non-separable Poisson equation Eq. (2) is based on  
 128 HOCS [13]. According to the mesh staggering, the HOCS derivatives from *cell-to-face*  $\delta_\xi^{cf}$   
 129 are given by:

$$\beta\phi'_{i-2} + \alpha\phi'_{i-1} + \phi'_i + \alpha\phi'_{i+1} + \beta\phi'_{i+2} = a \frac{\phi_{i+1/2} - \phi_{i-1/2}}{h_\xi} + b \frac{\phi_{i+3/2} - \phi_{i-3/2}}{3h_\xi} + c \frac{\phi_{i+5/2} - \phi_{i-5/2}}{5h_\xi} \quad (3)$$

130 whereas the *face-to-cell* derivative  $\delta_\xi^{cf}$  is given by the space-shift of the former relation:

$$\beta\phi'_{i-3/2} + \alpha\phi'_{i-1/2} + \phi'_{i+1/2} + \alpha\phi'_{i+3/2} + \beta\phi'_{i+5/2} = a \frac{\phi_{i+1} - \phi_i}{h_\xi} + b \frac{\phi_{i+2} - \phi_{i-1}}{3h_\xi} + c \frac{\phi_{i+3} - \phi_{i-2}}{5h_\xi} \quad (4)$$

131 The coefficients  $\alpha$ ,  $\beta$ ,  $a$ ,  $b$  and  $c$  are computed to ensure the constraints on the accuracy [13].  
 132 The HOCS discretizations used in this work are tabulated in the Tab. 1.

133 [Table 1 about here.]

134 For the periodic boundary conditions, these relations uniquely define the discretization of  
 135 the Poisson's equation Eq. (1). For the Neumann boundary conditions, lower-order up-  
 136 wind boundary relations are derived [13]. For instance, the following third-order boundary  
 137 conditions are considered [19]:

$$\phi'_{1/2} + 23\phi'_{3/2} = -25\phi_0 + 26\phi_1 - \phi_2 \quad (5)$$

138

$$\phi'_{1/2} - \phi'_{3/2} = -\phi_0 + 2\phi_1 - \phi_2 \quad (6)$$

139 Because of the implicit formulation of the compact schemes and the staggered grid, the linear  
 140 system arising from the HOCS discretization of Eq. (2) is no longer sparse. Solutions can  
 141 be computed by the successive diagonalization solver [10, 19, 27]. The non-separable feature

142 of the Poisson's equation Eq. (1) precludes this direct solver, and iterative ones remain a  
 143 natural way to consider. The present study focuses on the second-order finite differences  
 144 preconditioning of the non-separable Poisson's equation discretized with HOCS. According  
 145 to Haldenwang et al. [10], an eigenvalue analysis of the preconditioned Richardson iterations  
 146 method is investigated in the following.

147

## 148 2.2. Preconditioned Richardson iterations

149 The analysis of the second-order finite difference preconditioning for the HOCS discretiza-  
 150 tion of the Poisson equation relies on an eigenvalue analysis of the iteration matrix of the  
 151 Richardson method. This is motivated by the existence of several results for the convergence  
 152 rate estimates [10, 26]. The preconditioned Richardson iteration is defined by the sequence:

$$\phi^{(k+1)} = \phi^{(k)} - \omega H^{-1} r^{(k)}, \quad 0 \leq k \tag{7}$$

153 where  $\omega$  is a relaxation factor,  $r^k = L\phi^{(k)} - f$  denotes the residual at the iteration  $k$  and  $L$   
 154 stands for an HOCS discretization of Eq. (2). The notation  $H^{-1}$  refers to the preconditioning  
 155 method which is designed to ensure a good convergence of the sequence Eq. (7), and also  
 156 to be easily computed. Hence, a classical result is the derivation of the optimal relaxation  
 157 factor  $\omega_{opt}$  and convergence rate  $r_{opt}$ :

$$\omega_{opt} = 2/(\lambda_{max} + \lambda_{min}) \quad r_{opt} = (\lambda_{max} - \lambda_{min})/(\lambda_{max} + \lambda_{min}) \tag{8}$$

158 where  $\lambda_{min}$  and  $\lambda_{max}$  stand for the lowest and largest eigenvalues of the preconditioned prob-  
 159 lem  $H^{-1}L$ .

160 For the Poisson equation with a constant coefficient  $\kappa$  defined on a one-dimensional peri-  
 161 odic domain, a theoretical framework exists to derive the convergence rate from the precondi-  
 162 tioned Richardson method. Indeed, the eigenvectors of the second-order and the HOCS finite  
 163 differences Eq. (2) are similar. The eigenvectors are expressed as  $v_k = \exp(ik2\pi/n)$ ,  $1 \leq k \leq$   
 164  $n$ , and therefore the eigenvalues are derived from the Fourier analysis of the finite difference



165 schemes.  $H$  and  $L$  being respectively associated to the second-order finite difference and the  
 166 HOCS discretization of the one-dimensional version of Eq. (2), the discrete eigenvalues are  
 167 given by [13]:

$$\lambda_k(H) = \frac{\sin^2(w_k/2)}{4h^2}, \quad (9)$$

$$\lambda_k(L) = \frac{1}{4h^2} \left( \frac{a \sin(w_k/2) + b/3 \sin(3w_k/2) + c/5 \sin(5w_k/2)}{1 + 2\alpha \cos(w_k) + 2\beta \cos(2w_k)} \right)^2 \quad (10)$$

169 with  $w_k = 2k\pi/n$ . Since  $H$  and  $L$  share the same eigenvectors, the eigenvalues of the  
 170 preconditioned Poisson problem are determined by  $\lambda_k(H^{-1}L) = \lambda_k(L)/\lambda_k(H)$ . The Fig. 1  
 171 presents the eigenvalues  $\lambda_k(H^{-1}L)$  with respect to the HOCS listed in Tab. 1.

172 [Figure 1 about here.]

173 The curves in Fig. 1 show that the set of eigenvalues remains bounded by the values at the  
 174 limit of vanishing  $w = 0$  and at  $w = \pi$ :

$$\lambda_{min} = \left( \frac{a + b + c}{1 + 2\alpha + 2\beta} \right)^2, \quad \lambda_{max} = \left( \frac{a + b/3 + c/5}{1 + 2\alpha + 2\beta} \right)^2 \quad (11)$$

175 It should be noted that  $\lambda_{min} = 1$  because the accuracy requirement in the derivation of the  
 176 compact scheme needs to satisfy to  $1 + 2\alpha + 2\beta = a + b + c$  [13]. Thus, the condition number  
 177 of the preconditioned iteration matrix is determined by the maximal eigenvalue  $\lambda_{max}$ . In this  
 178 specific case, the estimation of the preconditioned Richardson's convergence rate is cleared-  
 179 up. Tab. (2) details the spectral radius, and the underlying optimal relaxation factor and  
 180 the convergence rate for the six schemes. (2).

181 [Table 2 about here.]

182 The eigenvalues of the preconditioned operator  $H^{-1}L$  are not dependent on the space size  
 183  $h$ . This result means that if the preconditioner  $H^{-1}$  scales like a multigrid method then the  
 184 higher-order accuracy is achieved with a linear complexity algorithmic because the HOCS  
 185 residual is itself computed with a linear algorithm complexity. The best convergence rate  
 186 holds for the fourth-order compact scheme *H4tri*, the worst holds for *H10pen*. The following

187 conclusion can be drawn: **the** more accurate is the scheme, the **worse** is the convergence.  
188 Thus, with the scheme *H10pen*, the convergence rate falls down to 0.29 which is less than  
189 two times more than the scheme *H4tri*. As indicated in the textbook of Canuto et al. [5] and  
190 observed by Abide et al. [28], the present analysis remains valid for multidimensional Pois-  
191 son’s equation. In the case of general Poisson equation, which involves a variable coefficient  
192 for instance, there is no exact derivation of the eigenvalues. Nevertheless, the eigenvalues of  
193 the preconditioned operator can be computed numerically. In the following, this procedure  
194 is considered as an alternative to the exact derivation.

195 The brute-force approach consists in assembling the matrices arising from the second-  
196 order and the HOCS discretizations  $H$  and  $L$ , and then to compute the eigenvalues. Clearly,  
197 this procedure depends on **the** mesh size  $N$ , excepted for the periodic case and **the** constant  
198 coefficient for which this approach is exact. For the other cases, a second-order conver-  
199 gence of the numerical error with respect to the mesh size  $N$  of the couple of eigenvalues  
200  $(\lambda_{min}, \lambda_{max})$  is observed (Fig. 2).

201 [Figure 2 about here.]

202 It is worth mentioning that the numerical error is computed from the reference eigenvalue  
203 computed with **the** finest mesh  $N = 256$ . The Fig. 2 presents the numerical errors **in** the  
204 three schemes *H4tri*, *H6tri* and *H6pen* with Neumann boundary conditions. A  $-2$  slope is  
205 noted, thus the Richardson extrapolation is considered to estimate the couple of extreme  
206 eigenvalues. The resulting data are presented in Tab. 3.

207 [Table 3 about here.]

208 It should be noted that the results are identical up to two digits. This procedure is considered  
209 hereinafter to assess the preconditioning for the variable coefficient case.

### 210 *2.3. Preconditioning with variable coefficients*

211 The second-order finite differences preconditioning is assessed for a variable coefficient  $\kappa$   
212 and both periodic and Neumann boundary conditions. Specifically, the two following variable

213 coefficients  $\kappa$  in Eq. (1) are considered:

$$\kappa_1(x) = 1 + \frac{9}{10} \sin(4\pi x) \quad (12)$$

$$\kappa_2(x) = \frac{2}{1 + \epsilon + (1 - \epsilon) \sin(4\pi x)} \quad (13)$$

214 where  $\epsilon$  is a parameter which defines the stiffness of the coefficient ( $\epsilon = 10^{-3}$ ). The coefficients  
215  $\kappa_1$ , and  $\kappa_2$  exhibit variations of  $O(1)$  and  $O(10^3)$  while being continuous. The Richardson  
216 extrapolation of the extreme eigenvalues for the preconditioned operator  $H^{-1}L$  is detailed  
217 in the Tab. 4.

218 [Table 4 about here.]

219 The eigenvalues are close to those derived with the constant coefficient assumption and dis-  
220 cussed in the section 2.2. Small discrepancies are observed especially with the stiff coefficient  
221  $\kappa_2$ . This can be attributed to an under-resolved mesh unable to describe the stiff variations  
222 of  $\kappa_2$ . A similar conclusion to the exact derivation of the convergence rate (Sec. 2.2) can be  
223 drawn: the spectral radius does not depend on the mesh size  $N$ . In addition no noticeable  
224 dependency on the coefficients  $\kappa$  is noted.

225 A similar analysis is carried out with the Neumann boundary conditions. Thus, the ex-  
226 treme eigenvalues are computed for the schemes *H4tri*, *H6tri* and *H6pen*. The results are  
227 presented in Tab. 5.

228 [Table 5 about here.]

229 The bounds of the eigenvalues are similar to those derived in the section (2.2) Eq. (11). The  
230 slight observed deviations can be explained by a coarse mesh which seems to be insufficient  
231 to describe the stiff variations of the coefficients  $\kappa$ .

232 To summarise the findings, the eigenvalues bound of the preconditioned operator  $H^{-1}L$  is  
233 not sensitive to the mesh size  $N$  [19]. Moreover, a finite difference preconditioning based on  
234 a variable coefficient Poisson equation leads also to an eigenvalue bound independent from  
235 the variable coefficient. This feature has two main consequences. First, this shows a way to

236 design a HOCS Poisson solver for non-separable problems **which could** not depend **on** the  
237 variable coefficient. **Secondly**, if the preconditioning step is efficiently performed, the method  
238 could benefit from High Performance Computing. It's because the HOCS residual can be also  
239 calculated with a linear algorithmic complexity while involving only halo exchange parallel  
240 communications [19].

#### 241 *2.4. Implementation*

242 The preconditioned Richardson sequence Eq. (7) relies on the evaluation of the HOCS  
243 residual Eq. (2) and on the solution of the second-order discretization of Eq. (1)  $H^{-1}$ . The  
244 evaluation of the preconditioning  $H^{-1}$  **has** to be performed efficiently to ensure correct overall  
245 performance. A review on **the** fast Poisson solver is proposed in the reference [4]. According  
246 to this review, FFT based solvers are among the most efficient for problems involving a  
247 constant coefficient. Otherwise, multigrid methods are shown to be suitable. Although,  
248 geometric multigrid methods are usually **more** efficient than algebraic multigrids for Poisson's  
249 equation on cubical domains [4], in this work, the AGMG library developed by Notay [1]  
250 is used. This choice is motivated by the user friendly interface, the black-box mode and  
251 its parallel implementation. It is worth mentioning **that** in each Richardson iteration of  
252 the sequence Eq. (7) only two or three iterations of the algebraic multigrid are performed.  
253 It has been experienced that only an approximate solving  $H^{-1}$  is sufficient to achieve the  
254 global convergence of the Richardson sequence. The method has been implemented using a  
255 previous parallel code dedicated to compact scheme discretizations [19].

### 256 **3. Numerical results**

257 This section is devoted to the assessment of the second-order finite difference precondi-  
258 tioning for a HOCS discretization of the non-separable Poisson equation. First the effective  
259 accuracy of the present solver implementation is demonstrated. Then, the extreme eigen-  
260 values are estimated from numerical experiments including numerical solution of Poisson's  
261 equation and the simulation of the unsteady natural convection in a tall cavity. This for-  
262 mer numerical experiment aims to illustrate the finite differences preconditioning in a more

263 general context.

### 264 3.1. HOCS accuracy verification

265 The accuracy of the HOCS discretizations for the problem Eq. (1) is verified. The method  
266 consists in computing the numerical error for several grid sizes in order to estimate the  
267 effective order of accuracy. A cubical domain is considered  $\Omega = [0, 2\pi]^3$ , with either periodic  
268 boundary or Neumann boundary conditions. The right-hand side of the Poisson equation is  
269 derived from the exact solution:

$$\phi = \cos(2\pi x) \cos(2\pi y) \cos(2\pi z) \quad (14)$$

270 and the following three-dimensional extensions of the coefficients Eq. (12) is considered:

$$\kappa_1 = 1 + \frac{9}{10} \sin(4\pi x) \sin(4\pi y) \sin(4\pi z) \quad (15)$$

$$\kappa_2 = \frac{2}{1 + \epsilon + (1 - \epsilon) \sin(4\pi x) \sin(4\pi y) \sin(4\pi z)} \quad (16)$$

271 The solutions are computed with the preconditioned Richardson sequence Eq. (7). In the  
272 case of Neumann boundary conditions the mesh is refined at the boundary according to  
273 a tangent hyperbolic mesh transformation [27]. Fig. 3 presents the numerical error with  
274 respect to the mesh size  $N$  for the coefficient  $\kappa_2$ .

275 [Figure 3 about here.]

276 Fig. 3-a shows that the numerical errors decrease linearly with the expected slopes. It is  
277 also noted that the numerical error for the scheme *H10pen* saturates beyond  $N = 64$  nodes  
278 because the machine accuracy is reached. Fig. 3-b corresponds to the Neumann boundary  
279 conditions. The slopes also agree with the expected HOCS's accuracy. These numerical  
280 experiments confirm that the present implementation of the preconditioned Richardson it-  
281 erations fulfils the accuracy requirements.

282 *3.2. Assessment of the preconditioning*

283 The validity of the spectral radius predictions established in the section 2 is verified  
 284 from the residual history of the Richardson iterations method. Indeed, the knowledge of the  
 285 convergence rate  $r_{opt}$  and the optimal relaxation factor  $\omega_{opt}$  allows us to estimate the couple  
 286 of extreme eigenvalues  $(\lambda_{min}, \lambda_{max})$  from the relations Eq. (8). The convergence rate  $r_{opt}$  is  
 287 computed from the residual slope [22]:

$$r = \sqrt[m_2 - m_1]{\frac{r_{m_1}}{r_{m_2}}} \quad (17)$$

288 where  $m_1, m_2$  denote two iteration numbers, and  $r_{m_1}, r_{m_2}$  the associated residual respectively.  
 289 The residual history is obtained from the zero solution of Poisson's equation and using a  
 290 random field as initial guess [22]. Fig. 4 presents the residuals for the scheme *H8tri*, the  
 291 variable coefficient  $\kappa_2$  with periodic boundary conditions.

292 [Figure 4 about here.]

293 First, it is observed that the convergence rate is slightly dependent on the mesh size  $N$ ,  
 294 but the slope reaches a limit as the mesh is refined. From the residual history observed  
 295 on the finest grid and using the relation Eq. (17), the convergence rate is estimated at  
 296  $r_{opt} = 0.29$ . It is worth mentioning that the relaxation factor of the Richardson sequences  
 297 Eq. (17) is initialized to the optimal value detailed in Tab. 2. In this case, the estimate of the  
 298 spectral bound for the preconditioned Richardson iterations is  $(\lambda_{min}, \lambda_{max}) = (1.01, 1.82)$ .  
 299 This result agrees with the eigenvalue analysis of the section 2. It should be noted that this  
 300 result validates the value of the optimal factor  $\omega_{opt}$ .

301 The sensitivity of the convergence rate evaluation to the mesh size is investigated. Fig. 5  
 302 presents the convergence rate  $r_{opt}$  with respect to the mesh size for the HOCS discretizations  
 303 and for the variable coefficient  $\kappa_2$ .

304 [Figure 5 about here.]

305 These curves show a small dependency on the convergence rate to the mesh size above grids  
 306 of size  $128^3$ . This result holds for both periodic and Neumann boundary conditions. This

307 confirms the main result of the section 2 which highlights that the convergence rate is not  
308 dependent on the mesh size, and thus, even if a stiff variable coefficient is **used**. In the  
309 following the convergence rate will be estimated from the finest grid  $256^3$ .

310 The spectral bounds of the iteration matrix is measured for each HOCS scheme. Tab. 6  
311 and Tab. 7 present the extreme eigenvalues  $(\lambda_{min}, \lambda_{max})$  computed from the residual curves on  
312 the finest grid  $256^3$ . First, for experiments involving periodic boundary conditions (Tab. 6),  
313 one can observed that for each discretization the couple of extreme eigenvalues are close to  
314 those predicted in the section 2.

315 [Table 6 about here.]

316 Thus, the minimal eigenvalue  $\lambda_{min}$  ranges **between** 1.00 and 1.02 while the expected value is  
317 1. Next, it is observed that the maximal eigenvalue  $\lambda_{max}$  is also close to the one predicted  
318 by the one-dimensional analysis developed in the section 2 (Tab. 2). This holds for the  
319 constant and **both** variable coefficients  $\kappa_1$  and  $\kappa_2$ . These numerical experiments corroborate  
320 the conclusion drawn in the section 2 on the properties of the second-order preconditioning:  
321 the independence of the convergence rate with respect to the mesh size and the coefficient  
322  $\kappa$ . The table 7 presents the two extreme eigenvalues in the case of prescribed Neumann  
323 boundary conditions.

324 [Table 7 about here.]

325 The computed eigenvalues are also similar to the prediction of the Tab. 2. This shows that  
326 despite the Neumann boundary conditions the eigenvalues spectra remains bounded.

327

328 **To illustrate the implications of this preconditioning on the wall time, the former is**  
329 **reported for several mesh sizes in table 8. Thus, the wall time is defined as the time necessary**  
330 **to decrease the residual to  $10^{-9}$  in case of a periodic domain, for the coefficient  $\kappa_2$  and with**  
331 **the scheme *H6tri*. In addition, the wall time of the multigrid AGMG preconditioner, and**  
332 **the wall time of the Conjugated Gradient to get the same level of residual are also reported.**

333

[Table 8 about here.]

First, one can note that the wall time of the multigrid preconditioning is almost the wall time of the preconditioned Richardson. This means that a higher accuracy is obtained at the cost of a second order discretization solved by a multigrid method. Since multigrid methods are known to scale linearly with the number of unknowns, it is expected that compact scheme discretizations of elliptic problems inherit of this scaling. Then, it is observed that the Conjugated Gradient perform well than preconditioned Richardson for coarser meshes than  $32^3$ . In other hand for finer meshes than  $32^3$ , it is the preconditioned Richardson which performs well. Indeed, in the absence of a preconditioning the number of iterations increases significantly with the problem size and the underlying ill-conditioning.

The present test confirms that the preconditioning is not sensitive to the Neumann/periodic boundary, to the mesh size and to the coefficient  $\kappa$ , at least for continuous one. However, these conclusions concern the model coefficients  $\kappa_1$  and  $\kappa_2$ . To extend the conclusions to more general coefficients, the simulation of a variable density flow is considered in the following.

### 3.3. Unsteady natural convection in a tall cavity

Let us consider the flow in a closed cavity with large temperature gradients. The low Mach number formulation of the Navier-Stokes equations may be considered as an alternative to the Boussinesq approximation for accounting buoyancy forces and density variations. A common way to address the simulations of such flow consists in solving a non-separable Poisson equation to enforce the final divergence of the velocity [20, 23]. This equation reads:

$$\nabla \cdot \frac{1}{\rho} \nabla \Phi = \nabla \cdot (\mathbf{u}^* - S) \quad (18)$$

where  $\Phi$  denotes the pressure-like variable,  $\mathbf{u}^*$  the provisional velocity,  $\rho$  the variable density and  $S$  the divergence to enforce. Knikker [20] proposed a detailed review of these approaches. In what follows, the denoted P1-A1 in [20] has been implemented with an in-house code devoted to the simulation of turbulent flows [28–30]. The velocity, pressure and temperature are located on a staggered grid, the time advancement is based on the semi-implicit Adams



359 Bashforth/Runge Kutta scheme and HOCS *H4tri*, *H6tri* and *H6pen* are considered. First,  
 360 the space accuracy of the present low Mach solver is demonstrated using the Method of  
 361 Manufactured Solutions [31]. According to the validation procedure of Bouloumou et al.  
 362 [32], the following two-dimensional analytical solution is considered:

$$\begin{aligned}
 u(x, y) &= +\cos x \sin y + \frac{1}{\text{Pr}\sqrt{\text{Ra}}} \cos x \sin y \\
 v(x, y) &= -\sin x \cos y + \frac{1}{\text{Pr}\sqrt{\text{Ra}}} \sin x \cos y \\
 p(x, y) &= \cos x \cos y \\
 T(x, y) &= 1 + \epsilon \sin x \sin y \\
 \rho(x, y) &= P_{th}/T(x, y) \\
 P_{th} &= 1
 \end{aligned}
 \tag{19}$$

363 with  $\text{Ra} = 10^3$ ,  $\text{Pr} = 0.71$  and  $\epsilon = 0.5$ . Both periodic and Dirichlet boundary conditions  
 364 (non-periodic) in a square computational domain  $\Omega = [0, 2\pi] \times [0, 2\pi]$  are considered. It  
 365 is worth mentioning that the analytical solution is a the non-solenoidal velocity field which  
 366 is specific to the low Mach model. The numerical error is computed with the L2-norm of  
 367 the difference between the exact and the numerical solution. The numerical error of the  
 368 pressure  $p$  is reported in the figure 6 for each discretization *H4*, *H6tri* and *H6pen*. For the  
 369 sake of clarity, the analysis based on the velocity and on the temperature are not reported  
 370 because of the numerical error slopes are similar to the pressure one.

371 [Figure 6 about here.]

372 The slopes of the numerical error show the fourth and the sixth-order accuracy of the imple-  
 373 mented code for periodic boundary conditions (Fig. 6). The same conclusion holds for the  
 374 non-periodic conditions with a slightly above slope that the expected one. For instance, the  
 375 slopes of 5.7 and 5.6 are noted for the tridiagonal and pentadiagonal sixth-order compact  
 376 schemes.

377 In addition, the present low Mach solver is validated against the steady natural convection

378 flow in a differentially heated cavity with a large temperature gradient. The configuration  
379 flow is detailed in the Benchmark [6]. The control flow parameters are the Rayleigh num-  
380 ber, the deviation to the Boussinesq approximation set to  $\epsilon = 0.6$  and the Prandlt number  
381  $Pr = 0.71$ . The thermophysical properties are constant. A grid sensitivity analysis is  
382 performed to assess the accuracy of the present low Mach solver at the Rayleigh number  
383  $Ra = 10^5$ . First, a fine grid solution has been computed on a mesh of size  $120 \times 120$  and  
384 with the small CFL number 0.05. This simulation leads to a Nusselt number  $Nu = 4.5516$   
385 and a thermodynamic pressure  $P_{th}/P_0 = 0.8518$ , which agrees the values computed in [32]  
386 and [33]. Fig. 7 presents, for the grid sizes  $N = 32, 48$  and  $64$ , the absolute difference with  
387 the fine grid solution of the Nusselt number and thermodynamic pressure.

388 [Figure 7 about here.]

389 The slopes confirm the expected accuracy, and even show a saturation due to the low level  
390 error for the two sixth-order schemes. A further validation is performed with a higher  
391 Rayleigh number  $Ra = 10^6$ . For a mesh of size  $128 \times 128$ , the computed Nusselt number  
392 is  $Nu = 8.8598$  and the final thermodynamic pressure  $P_{th}/P_0 = 0.856338$ , which agree well  
393 with the reference solution [6]. Fig. 8 presents the streamlines and the isolines of the  
394 temperature.

395 [Figure 8 about here.]

396 Both plots are in agreement with the results of Heuveline [34]. The present low Mach  
397 solver implementation being validated, one can focus on the spectrum of the finite difference  
398 preconditioning.

399 To this end, the unsteady natural convection in a tall cavity is considered [35, 36]. The  
400 aspect ratio of the cavity is 1:8, the Rayleigh number is  $Ra = 10^6$  and the normalized  
401 temperature difference is  $\epsilon = 0.8$ . This former parameter is sufficiently high to lead to a  
402 strongly unsteady flow with large density variations: the order of magnitude is one. The  
403 simulations of the flow are carried out up to a dimensionless time  $t = 1000$  with a CFL  
404 number of 0.8 and using a fine mesh  $128 \times 512$ . Fig. 9 presents a temporal snapshot sequence  
405 of the isolines of temperature.

406 [Figure 9 about here.]

407 The contours plots agree qualitatively with those recently published [35, 36]. The convergence  
408 rate of the Richardson iterations sequence is measured for the three discretizations *H4tri*,  
409 *H6tri* and *H6pen* using the procedure detailed in the section 3.2. Thus, the maximum of the  
410 residual Eq. (7) with respect to the Richardson iteration number *it* is plotted in Fig. 10 for  
411 one temporal iteration of the Navier-Stokes solver. It should be mentioned that the iterative  
412 procedure Eq. (7) has been initialized with  $\phi = 0$  and was stopped when the residual is  
413 below  $\|r\| < 10^{-10}$ .

414 [Figure 10 about here.]

415 Also, it has been observed that whatever the time step the slopes of Fig. (8), the curves  
416 remain of similar slope. This observation confirms that a such low-order preconditioning is  
417 not sensitive to the variable coefficient  $\rho$ . For this mesh size, the solution of time of the  
418 pressure equation is about 1.1 s with 24 processors. The measured convergence rates on  
419 Fig. (8) and the associated *extrem* eigenvalues are summarized in Tab. 9.

420 [Table 9 about here.]

421 The *assessed extrem* eigenvalues agree the theoretical estimates of the section 2. It should  
422 be noticed that the spectrum of the preconditioned operator is slightly smaller. This can  
423 be explained by the cancellation of the high-frequency fluctuations due to the fine mesh or  
424 the compact schemes cut-off [13]. This test confirms that the second-order finite difference  
425 preconditioning of HOCS compact schemes for non-separable Poisson's equation possess a  
426 bounded spectrum independent to the variable coefficient.

#### 427 4. Conclusion

428 An analysis of the second-order finite-difference preconditioning of the higher-order  
429 compact scheme discretization regarding the variable coefficient Poisson equation is pre-  
430 sented in this work. In particular, it is demonstrated that the preconditioner built from the

431 second-order finite-difference discretization leads to an iterative Richardson method that the  
432 convergence rate is not sensitive to the mesh size and the variable coefficient. The finding  
433 is even more valuable that this preconditioning can be applied on the conservative form of  
434 the Poisson's equation, the one involved in some discretizations of variable density flows for  
435 instance.

436 Several numerical experiments based on manufactured solutions demonstrate the accu-  
437 racy of the discretization up to the tenth-order. The convergence rate of the present lower-  
438 order preconditioned Richardson method has been found not sensitive to the mesh-size and  
439 the variable coefficient. This former finding is verified with a more general variable-coefficient  
440 test case: variable density flow occurring in a strongly heated cavity. This demonstrates the  
441 relevance of the lower-order preconditioning for the compact scheme discretizations even the  
442 more that the present solver involves numerical methods with linear computational complex-  
443 ity.

444 Further investigations would to put forward a such low-order preconditioning as a simple  
445 way to achieve simultaneously scalable algorithm and higher-order accuracy, and thus to  
446 take full advantage of the High Performance Computing.

447

## 448 **Acknowledgements**

449 The project has received funding from the European Union's Horizon 2020 Research and  
450 Innovation Programme under the Marie Skłodowska-Curie grant agreement No. 823731 -  
451 CONMECH. This work was also realized with the support of HPC@LR, a Center of compe-  
452 tence in High-Performance Computing from the Languedoc-Roussillon region.

## 453 **References**

454 [1] Y. Notay, An aggregation-based algebraic multigrid method, *Electronic transactions*  
455 *on numerical analysis* 37 (2010) 123–146.

- 456 [2] A. H. Baker, R. D. Falgout, T. V. Kolev, U. M. Yang, Scaling hypre's multigrid solvers to  
457 100,000 cores, in: High-Performance Scientific Computing, Springer, 2012, pp. 261–279.
- 458 [3] P. R. Amestoy, I. S. Duff, J. Koster, J.-Y. L'Excellent, A fully asynchronous multifrontal  
459 solver using distributed dynamic scheduling, SIAM Journal on Matrix Analysis and  
460 Applications 23 (2001) 15–41.
- 461 [4] A. Gholami, D. Malhotra, H. Sundar, G. Biros, FFT, FMM, or Multigrid? a compar-  
462 ative study of state-of-the-art Poisson solvers for uniform and nonuniform grids in the  
463 unit cube, SIAM Journal on Scientific Computing 38 (2016) C280–C306.
- 464 [5] C. Canuto, A. Quarteroni, M. Hussaini, T. Zang, Spectral method in fluid mechanics,  
465 Springer-Verlag, New York, 1988.
- 466 [6] P. Le Quéré, C. Weisman, H. Paillère, J. Vierendeels, E. Dick, R. Becker, M. Braack,  
467 J. Locke, Modelling of natural convection flows with large temperature differences: a  
468 benchmark problem for low Mach number solvers. part 1. reference solutions, ESAIM:  
469 Mathematical Modelling and Numerical Analysis 39 (2005) 609–616.
- 470 [7] O. Botella, R. Peyret, Benchmark spectral results on the lid-driven cavity flow, Com-  
471 puters & Fluids 27 (1998) 421–433.
- 472 [8] D. Pekurovsky, P3DFFT: A framework for parallel computations of Fourier transforms  
473 in three dimensions, SIAM Journal on Scientific Computing 34 (2012) C192–C209.
- 474 [9] S. A. Orszag, Spectral methods for problems in complex geometrics, Elsevier, 1979.
- 475 [10] P. Haldenwang, G. Labrosse, S. Abboudi, M. Deville, Chebyshev 3-d spectral and 2-d  
476 pseudospectral solvers for the Helmholtz equation, Journal of Computational Physics  
477 55 (1984) 115–128.
- 478 [11] G. Labrosse, A. Redondo, The optimal 3-node preconditioner of the d2dx2 Fourier and  
479 Chebyshev spectral operators, Journal of Computational Physics 230 (2011) 147–158.

- 480 [12] L. Collatz, The numerical treatment of differential equations, 1966.
- 481 [13] S. K. Lele, Compact finite difference schemes with spectral-like resolution, *Journal of*  
482 *computational physics* 103 (1992) 16–42.
- 483 [14] P. C. Chu, C. Fan, A three-point combined compact difference scheme, *Journal of*  
484 *Computational Physics* 140 (1998) 370–399.
- 485 [15] W. F. Spitz, G. F. Carey, A high-order compact formulation for the 3d Poisson equation,  
486 *Numerical Methods for Partial Differential Equations: An International Journal* 12  
487 (1996) 235–243.
- 488 [16] M. M. Gupta, J. Zhang, High accuracy multigrid solution of the 3d convection–diffusion  
489 equation, *Applied Mathematics and Computation* 113 (2000) 249–274.
- 490 [17] A. C. Medina, R. Schmid, Solution of high order compact discretized 3d elliptic partial  
491 differential equations by an accelerated multigrid method, *Journal of Computational*  
492 *and Applied Mathematics* 350 (2019) 343–352.
- 493 [18] S. Abide, X. Chesneau, B. Zeghamati, Compact mixed methods for convection/diffusion  
494 type problems, *Applied Mathematics and Computation* 218 (2012) 5867–5876.
- 495 [19] S. Abide, B. Zeghamati, Multigrid defect correction and fourth-order compact scheme for  
496 Poisson’s equation, *Computers & Mathematics with Applications* 73 (2017) 1433–1444.
- 497 [20] R. Knikker, A comparative study of high-order variable-property segregated algorithms  
498 for unsteady low Mach number flows, *International Journal for Numerical Methods in*  
499 *Fluids* 66 (2011) 403–427.
- 500 [21] A. Brüger, B. Gustafsson, P. Lötstedt, J. Nilsson, High order accurate solution of the  
501 incompressible Navier-Stokes equations, *Journal of Computational Physics* 203 (2005)  
502 49–71.
- 503 [22] U. Trottenberg, C. W. Oosterlee, A. Schuller, *Multigrid*, Elsevier, 2000.

- 504 [23] F. Nicoud, Conservative high-order finite-difference schemes for low-Mach number flows,  
505 Journal of Computational Physics 158 (2000) 71–97.
- 506 [24] M. S. Dodd, A. Ferrante, A fast pressure-correction method for incompressible two-fluid  
507 flows, Journal of Computational Physics 273 (2014) 416–434.
- 508 [25] E. Motheau, J. Abraham, A high-order numerical algorithm for dns of low-Mach-  
509 number reactive flows with detailed chemistry and quasi-spectral accuracy, Journal of  
510 Computational Physics 313 (2016) 430–454.
- 511 [26] P. Concus, G. H. Golub, Use of fast direct methods for the efficient numerical solution  
512 of nonseparable elliptic equations, SIAM Journal on Numerical Analysis 10 (1973)  
513 1103–1120.
- 514 [27] S. Abide, S. Viazzo, A 2d compact fourth-order projection decomposition method,  
515 Journal of Computational Physics 206 (2005) 252–276.
- 516 [28] S. Abide, M. Binous, B. Zeghmami, An efficient parallel high-order compact scheme for  
517 the 3d incompressible Navier-Stokes equations, International Journal of Computational  
518 Fluid Dynamics 31 (2017) 214–229.
- 519 [29] H. Doukkali, S. Abide, M. Lhassane Lahlaouti, A. Khamlichi, Large eddy simulation of  
520 turbulent natural convection in an inclined tall cavity, Numerical Heat Transfer, Part  
521 A: Applications (2018) 1–15.
- 522 [30] S. Abide, S. Viazzo, I. Raspo, A. Randriamampianina, Higher-order compact scheme  
523 for high-performance computing of stratified rotating flows, Computers & Fluids 174  
524 (2018) 300–310.
- 525 [31] P. J. Roache, Code verification by the method of manufactured solutions, J. Fluids  
526 Eng. 124 (2002) 4–10.

- 527 [32] O. Bouloumou, E. Serre, P. Bontoux, J. Fröhlich, A 3d pseudo-spectral low mach-  
528 number solver for buoyancy driven flows with large temperature differences, *Computers  
529 & fluids* 66 (2012) 107–120.
- 530 [33] G. Accary, I. Raspo, A 3d finite volume method for the prediction of a supercritical fluid  
531 buoyant flow in a differentially heated cavity, *Computers & fluids* 35 (2006) 1316–1331.
- 532 [34] V. Heuveline, On higher-order mixed fem for low Mach number flows: application to a  
533 natural convection benchmark problem, *International Journal for Numerical Methods  
534 in Fluids* 41 (2003) 1339–1356.
- 535 [35] A. Tyliczszak, High-order compact difference algorithm on half-staggered meshes for  
536 low Mach number flows, *Computers & Fluids* 127 (2016) 131–145.
- 537 [36] Y.-L. Feng, S.-L. Guo, W.-Q. Tao, P. Sagaut, Regularized thermal lattice Boltzmann  
538 method for natural convection with large temperature differences, *International Journal  
539 of Heat and Mass Transfer* 125 (2018) 1379–1391.



540 **List of Figures**

541	1	Eigenvalues of the preconditioned problem $H^{-1}L$ for several HOCS discretizations. . . . .	25
542			
543	2	Mesh convergence of the spectral radius of $H^{-1}L$ : Neumann boundary conditions and constant coefficient. . . . .	26
544			
545	3	Assessment of the order of accuracy: variable coefficient $\kappa_2$ . . . . .	27
546	4	Mesh sensitivity of the residual history: periodic domain and coefficient $\kappa_2$ . .	28
547	5	Mesh sensitivity of the convergence rate: periodic domain and coefficient $\kappa_2$ . .	29
548	6	The numerical errors of the pressure variable. . . . .	30
549	7	Grid sensitivity analysis of the differentially heated cavity at $Ra = 10^5$ . . . .	31
550	8	Natural convection in a square cavity: $(Ra, \epsilon, Pr) = (10^6, 0.6, 0.71)$ and constant properties. . . . .	32
551			
552	9	Snapshots of 15 isolines of temperature ranging in 0.3 and 1.7: $(Ra, \epsilon, Pr) = (10^6, 0.8, 0.71)$ . . . . .	33
553			
554	10	Natural convection in the tall cavity: residual history of the preconditioned Richardson iteration. . . . .	34
555			

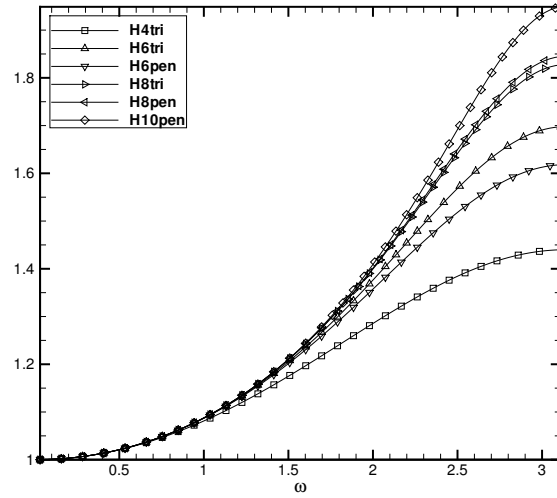


Figure 1: Eigenvalues of the preconditioned problem  $H^{-1}L$  for several HOCS discretizations.

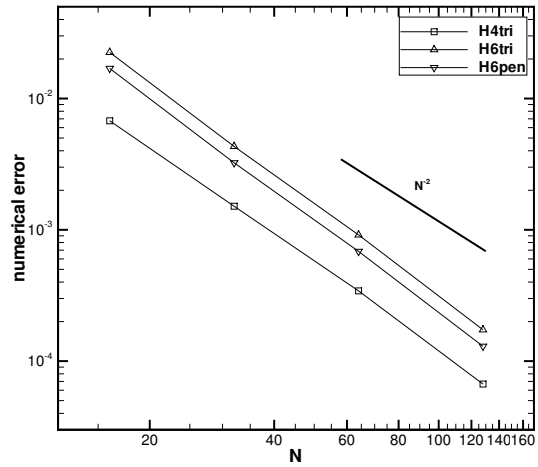
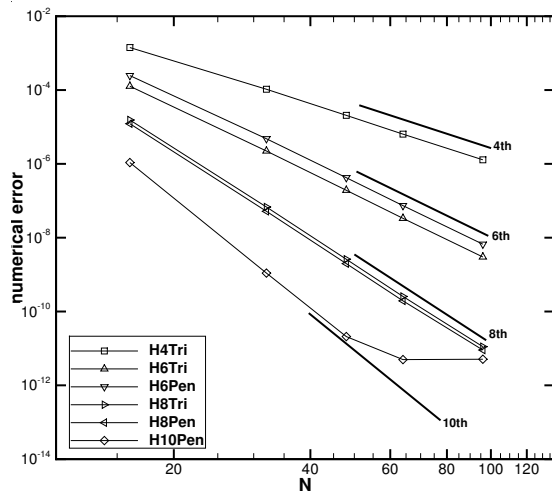
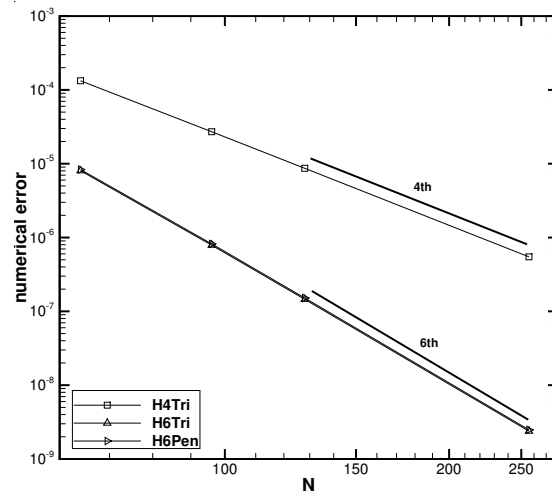


Figure 2: Mesh convergence of the spectral radius of  $H^{-1}L$ : Neumann boundary conditions and constant coefficient.



(a) Periodic BCs



(b) Neumann BCs

Figure 3: Assessment of the order of accuracy: variable coefficient  $\kappa_2$ .

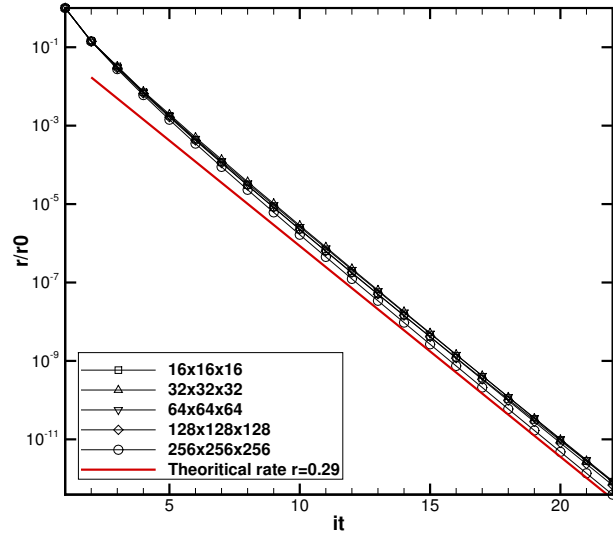


Figure 4: Mesh sensitivity of the residual history: periodic domain and coefficient  $\kappa_2$ .

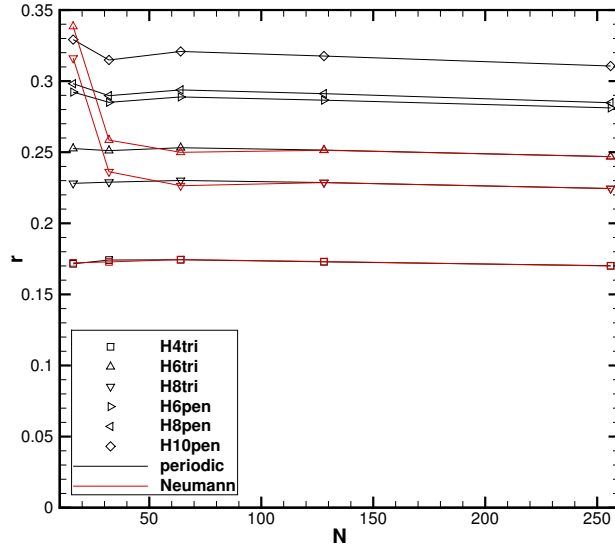


Figure 5: Mesh sensitivity of the convergence rate: periodic domain and coefficient  $\kappa_2$ .

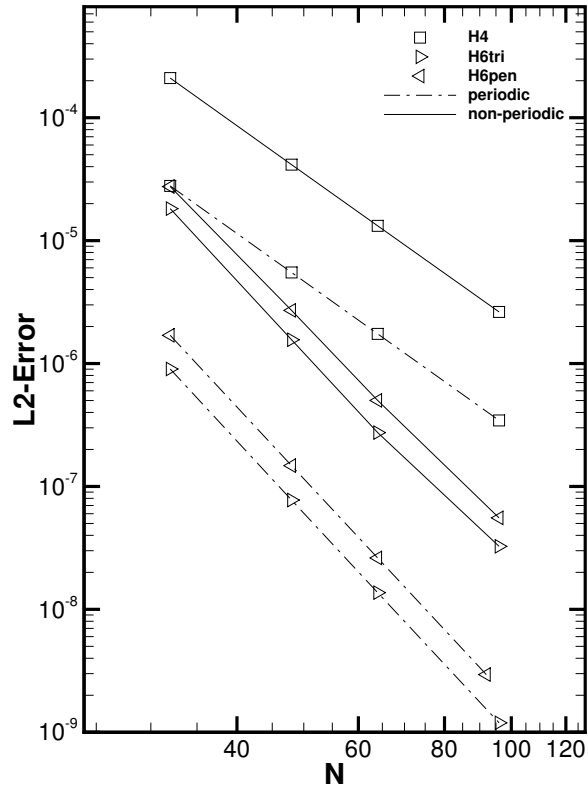


Figure 6: The numerical errors of the pressure variable.

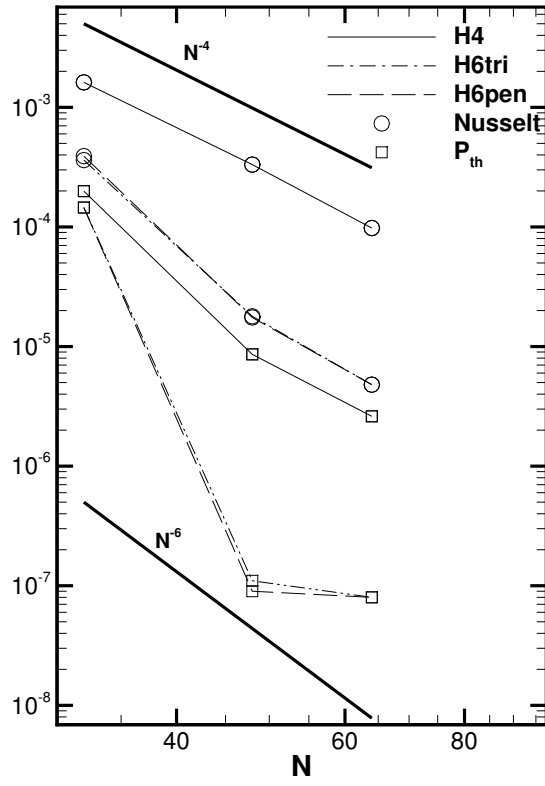
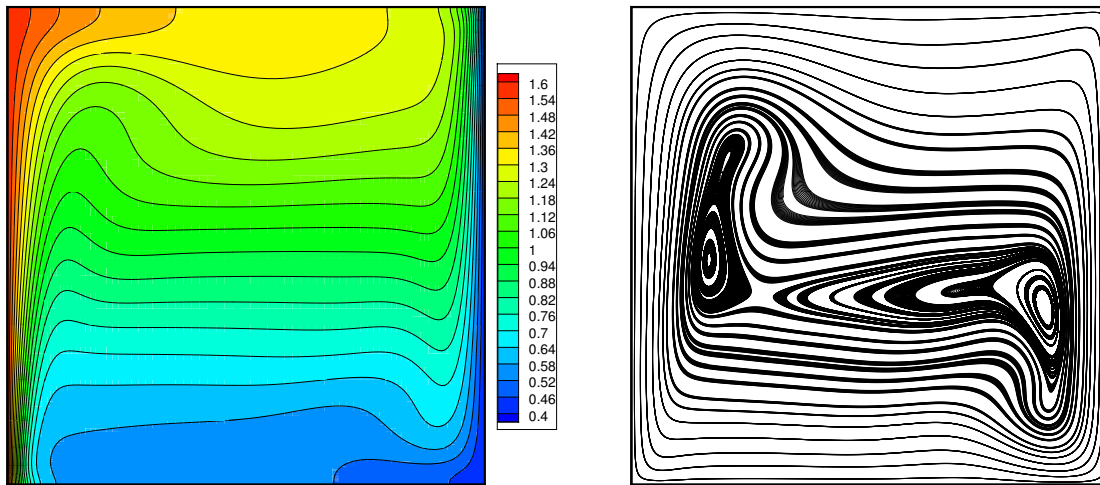


Figure 7: Grid sensitivity analysis of the differentially heated cavity at  $Ra = 10^5$ .





(a) Isolines of temperature

(b) Streamlines

Figure 8: Natural convection in a square cavity:  $(Ra, \epsilon, Pr) = (10^6, 0.6, 0.71)$  and constant properties.

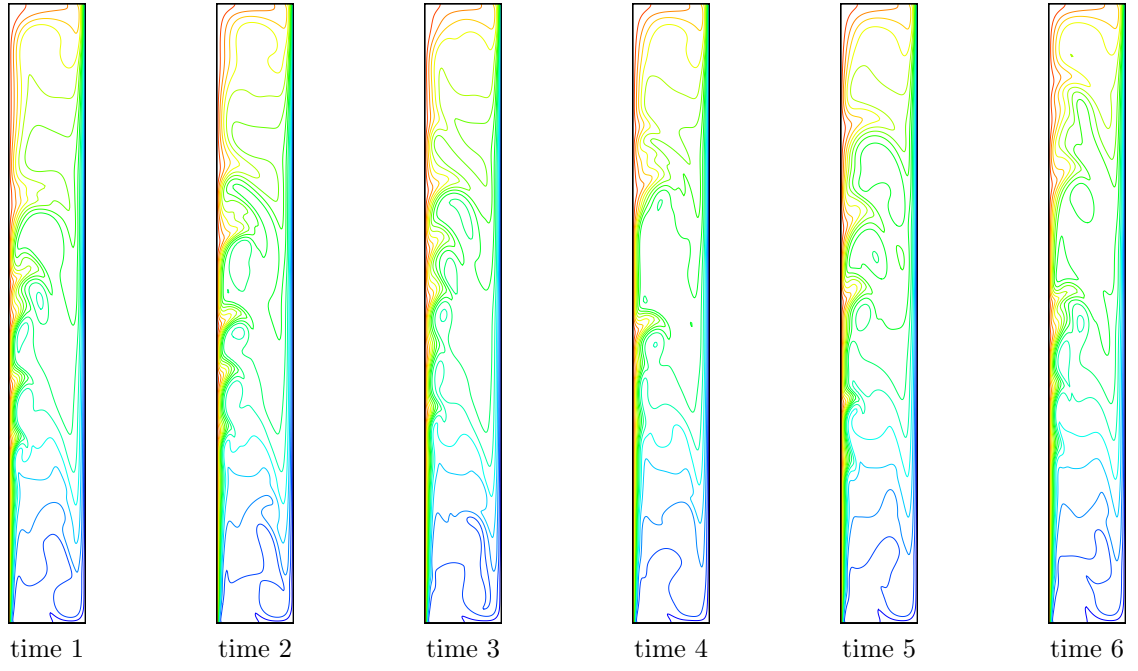


Figure 9: Snapshots of 15 isolines of temperature ranging in 0.3 and 1.7:  $(Ra, \epsilon, Pr) = (10^6, 0.8, 0.71)$ .

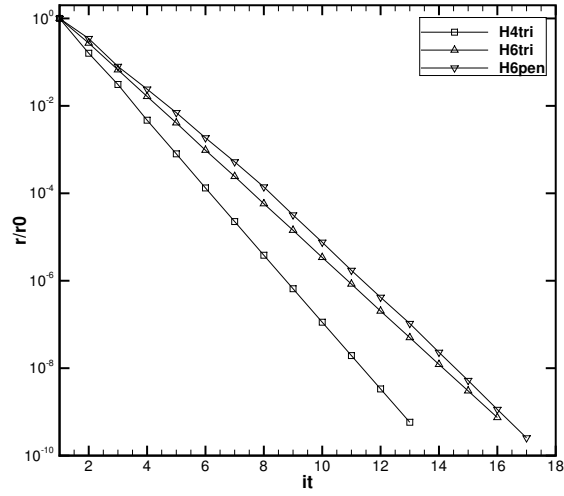


Figure 10: Natural convection in the tall cavity: residual history of the preconditioned Richardson iteration.

556 **List of Tables**

557	1	Compact scheme coefficients for the first derivative defined on a staggered grid.	36
558	2	The lowest and largest eigenvalues of the preconditioned operator $H^{-1}L$ and	
559		the underlying optimal parameters for the preconditioned Richardson iterations.	37
560	3	The lowest and largest eigenvalues of the preconditioned Richardson method:	
561		Neumann boundary conditions and constant coefficient. . . . .	38
562	4	The lowest and largest eigenvalues of the preconditioned Richardson method:	
563		periodic boundary conditions and variable coefficient. . . . .	39
564	5	The lowest and largest eigenvalues of the preconditioned Richardson method:	
565		Neumann boundary conditions and variable coefficient. . . . .	40
566	6	Estimates of the lowest and largest eigenvalues of the preconditioned Richard-	
567		son method: periodic boundary conditions and variable coefficient. . . . .	41
568	7	Lowest and largest eigenvalues estimates of the preconditioning : Neumann	
569		boundary conditions and variable coefficient. . . . .	42
570	8	Wall time in second to solve the Poisson equation with the variable coefficient	
571		$\kappa_2$ . Notations: Conjugate Gradient (CG), Richardson preconditioned (PR)	
572		by the algebraic multigrid AGMG. . . . .	43
573	9	Estimates of the textcolorblueextrem eigenvalues evaluated from the simula-	
574		tion of the tall cavity flow. . . . .	44

name	order	$\alpha$	$\beta$	$a$	$b$	$c$
H4tri	$h^4$	1/22	0	12/11	0	0
H6tri	$h^6$	9/62	0	63/62	17/62	0
H6pen	$h^6$	154/1289	-17/5178	960/863	0	0
H8tri	$h^8$	25/118	0	2675/2832	925/1888	-61/5664
H8pen	$h^8$	6114/25669	183/51338	23400/25669	14680/25669	0
H10pen	$h^{10}$	96850/288529	9675/577058	683425/865587	505175/577058	69049/1731174

Table 1: Compact scheme coefficients for the first derivative defined on a staggered grid.

scheme	H4tri	H6tri	H6pen	H8tri	H8pen	H10pen
$\lambda_{min}$	1.00	1.00	1.00	1.00	1.00	1.00
$\lambda_{max}$	1.44	1.70	1.62	1.83	1.84	1.95
$r_{opt}$	0.18	0.26	0.24	0.29	0.30	0.32
$\omega_{opt}$	0.82	0.74	0.76	0.71	0.70	0.68

Table 2: The lowest and largest eigenvalues of the preconditioned operator  $H^{-1}L$  and the underlying optimal parameters for the preconditioned Richardson iterations.

scheme	H4tri	H6tri	H6pen
$\lambda_{min}$	1.00	1.00	1.00
$\lambda_{max}$	1.44	1.70	1.62

Table 3: The lowest and largest eigenvalues of the preconditioned Richardson method: Neumann boundary conditions and constant coefficient.

case	scheme	H4tri	H6tri	H6pen	H8tri	H8pen	H10pen
$\kappa_2$	$\lambda_{min}$	1.00	1.00	1.00	1.00	1.00	1.00
$\kappa_2$	$\lambda_{max}$	1.44	1.70	1.62	1.83	1.85	1.95
$\kappa_3$	$\lambda_{min}$	0.99	0.99	0.99	0.99	0.99	0.99
$\kappa_3$	$\lambda_{max}$	1.45	1.70	1.62	1.83	1.85	1.95

Table 4: The lowest and largest eigenvalues of the preconditioned Richardson method: periodic boundary conditions and variable coefficient.



case	scheme	H4tri	H6tri	H6pen
$\kappa_1$	$\lambda_{min}$	1.00	0.98	1.00
	$\lambda_{max}$	1.44	1.70	1.62
$\kappa_2$	$\lambda_{min}$	1.00	0.99	0.99
	$\lambda_{max}$	1.45	1.72	1.64

Table 5: The lowest and largest eigenvalues of the preconditioned Richardson method: Neumann boundary conditions and variable coefficient.

case	scheme	H4tri	H6tri	H6pen	H8tri	H8pen	H10pen
constant	$\lambda_{min}$	1.01	1.02	1.02	1.02	1.02	1.02
	$\lambda_{max}$	1.43	1.68	1.60	1.81	1.82	1.93
$\kappa_1$	$\lambda_{min}$	1.00	1.02	1.01	1.01	1.02	1.02
	$\lambda_{max}$	1.44	1.68	1.61	1.81	1.82	1.93
$\kappa_2$	$\lambda_{min}$	1.01	1.01	1.01	1.01	1.01	1.01
	$\lambda_{max}$	1.43	1.69	1.61	1.82	1.84	1.94

Table 6: Estimates of the lowest and largest eigenvalues of the preconditioned Richardson method: periodic boundary conditions and variable coefficient.

case	scheme	H4tri	H6tri	H6pen
constant	$\lambda_{min}$	1.01	1.01	1.02
	$\lambda_{max}$	1.43	1.68	1.60
$\kappa_1$	$\lambda_{min}$	1.01	1.02	1.01
	$\lambda_{max}$	1.43	1.68	1.61
$\kappa_2$	$\lambda_{min}$	0.98	1.01	0.99
	$\lambda_{max}$	1.46	1.69	1.63

Table 7: Lowest and largest eigenvalues estimates of the preconditioning : Neumann boundary conditions and variable coefficient.

$N$	CG	AGMG	PR
$16^3$	0.02	0.43	0.47
$32^3$	0.42	1.69	1.96
$48^3$	4.64	3.54	3.80
$64^3$	17.42	8.33	8.99
$96^3$	247.80	23.00	25.61

Table 8: Wall time in second to solve the Poisson equation with the variable coefficient  $\kappa_2$ . Notations: Conjugate Gradient (CG), Richardson preconditioned (PR) by the algebraic multigrid AGMG.

scheme	H4tri	H6tri	H6pen
$r$	0.17	0.24	0.23
$\lambda_{min}$	1.01	1.02	1.01
$\lambda_{max}$	1.43	1.68	1.61

Table 9: Estimates of the extrem eigenvalues evaluated from the simulation of the tall cavity flow.